SLAT NOISE PREDICTIONS BASED ON APE AND STOCHASTIC SOUND SOURCES FROM RANS

R. Ewert, M. Münsch
Deutsches Zentrum für Luft- und Raumfahrt e.V.
Institut für Aerodynamik und Strömungstechnik
Abteilung Technische Akustik
Lilienthalplatz 7, 38108 Braunschweig / Germany

Keywords: *CAA,APE,RPM,Slat Noise*

Abstract

Slat Noise simulations are carried out for a high-lift airfoil. A low-cost Computational Aeroacoustics (CAA) approach is applied, which is based on acoustic perturbation equations (APE) in the time-domain that are forced by stochastic sound sources. The newly developed stochastic model is based on the spatial convolution of white-noise and reproduces very accurately target distributions of turbulence kinetic energy and length scales as provided by a steady RANS computation of the turbulent flow problem. The method is applied to simulate spectra and directivities of the slat noise problem. The Mach number scaling law of the broadband slat noise component is evaluated based on three different freestream velocities (M=0.088, 0.118, 0.165). The acoustic benefit of a slat cove cover on broadband sound generation is numerically studied.

1 Introduction

The noise levels of modern jet engines are significantly lowered due to the introduction of high bypass ratios. Today, airframe noise can be identified as an equally intensive noise source during the landing approach of transport aircraft. In particular, experimental studies have identified deployed slats as prominent contributors to the over-all sound pressure levels of aircraft [2, 16].

To reduce noise emissions further, numerical tools will become crucial in the future to directly assist the design of low-noise airframe components.

In the last years numerical techniques have been developed in the framework of Computational Aeroacoustics (CAA) to simulate on volume meshes wave propagation through moving fluids. For example, high-order non-dispersive spatial and temporal discretization schemes and high-quality non-reflecting boundary conditions have been proposed. However, to apply CAA techniques in a design cycle to airframe noise problems two additional points have to be considered. Firstly, to be useful in a design procedure a potential computational method has to have a short computational time that allows to study a large number of geometrical modifications in a meaningful time frame. Secondly, a characteristic feature of airframe noise, besides the wave-propagation through non-uniform air and the interaction of waves with complex geometries, is the involvement of turbulent flow as the primarily cause of broadband sound radiation. Concerning the prediction of broadband airframe noise, a pure propagation tool is useless unless the turbulent sound sources are appropriately specified and incorporated into the method.

The highest physical level of description of the unsteady turbulent flow problem, can be achieved by means of a direct numerical simulation (DNS). A less detailed, but for techni-

cal purposes presumably sufficient resolution of the turbulent flow problem can be achieved via Large Eddy Simulation (LES). Unlike the DNS approach, the LES does not resolve the full turbulent flow problems but rather splits the flow problem into resolved large scale turbulent structures and subgrid scales, whose influence on the resolved scales are appropriately modeled.

In the hybrid aeroacoustic approach, unsteady acoustic sources of the propagation equations are computed from LES or DNS simulations, respectively. Such an approach, however, has an overall computational time orders of magnitudes too high to be considered useful in a design process. On the contrary, any significant reduction of the computational time must notabene involve a higher degree of modeling compared to a DNS or LES approach.

In this paper the sound generation at the slat of a two element high-lift configuration is studied using a cheaper computational approach that involves CAA techniques in conjunction with stochastic sound sources in the time domain. The stochastic approach to set up turbulent velocity fluctuations is based on a steady Reynolds averaged Navier Stokes (RANS) simulation of the turbulent flow problem, which provides in case of a two equation turbulence closure informations about local values of the turbulence kinetic energy and the integral length scale of turbulence. The simplifications inherent in this approach are due to the approximative turbulence closure used for RANS that yields an approximative solution of the time averaged turbulent flow problem. Furthermore, spatial correlation functions (and thus implicitly the shape of turbulence spectra) have to be modeled since RANS provides no details about this turbulence feature.

In general the resolution requirements for an unsteady LES (which is determined by the smallest eddy size resolved to achieve an accurate simulation) do not necessarily coincide with those needed for an aeroacoustic simulation related to the same problem (which is determined by a highest acoustic frequency of interest). For the slat geometry studied in this paper, LES and acoustic resolution requirements differ in at least one order of magnitude: the smallest eddies to be resolved by LES can be estimated to generate frequencies up to 400kHz, whereas the highest acoustic frequency of interest is about 10kHz. In other words, although the stochastic modeling of turbulent unsteady sources usually demands to have a higher CAA mesh resolution in the near field area where sources have to be resolved, the resolution requirements are for each spatial direction about one order of magnitude less stringent than those of a highly accurate LES simulation to solve the turbulent flow problem. Furthermore, major savings in computational time are due to the small computational effort involved to set up unsteady stochastic fluctuations in comparison to the effort a full LES simulation needs. Slat noise computations benefit from the fact that a 2D simulation is possible for this cylindrical problem, with a 2D to 3D correction applied afterwards. A LES simulation always has to solve the full 3D turbulent flow problem.

The reduction of computational time can be estimated to reach approximately three orders of magnitude for the stochastic approach compared to a conventional LES, such that the use as a design tool becomes feasible.

In Refs. [5, 4] a Random Particle Mesh (RPM) method was introduced as a new stochastic technique to generate broadband sound sources in the time-domain. The method is based on the spatial filtering of random white-noise. It reproduces first- and second-order one- and two-point statistics. In particular, in case of homogeneous isotropic turbulence it is possible to reproduce exactly the complete second-order two-point velocity correlation tensor [1].

The new stochastic method has some advantages over classical stochastic approaches in aeroacoustics that are based on random Fourier modes, following the early work of Kraichnan [11]. It is time- and memory-efficient, strictly solenoidal, and can easily be applied to highly non-uniform mean-flows, e.g., in the slat-cove of a high-lift airfoil. The method reproduces very accurately the target distribution of turbulence kinetic energy and length scales as provided by the steady RANS simulation. Furthermore, it avoids

the occurrence of shear decorrelations and resolves broadband spectra continuously.

This paper is organized as follows. The computational problem is introduced in Section 2. Acoustic simulation techniques are are discussed in Section 3. Section 4 discusses the computational results for the two-element airfoil configuration. Finally, conclusions are drawn in Section 5.

2 Computational Problem

Slat noise simulations are carried out for a modified two-element high-lift configuration, which consists of a slat and a main-element. Fig. 1 shows the airfoil section used for the simulations. The slat geometry and the main-element correspond up to 40% chord length to the geometry of a representative three-element high-lift configuration. The remaining part of the main-element is modified by increasing the camber to aerodynamically compensate for the omitted flap. The geometrical design was developed in the German project FREQUENZ that aims at studying design modifications at three selected aeroacoustic problems numerically and experimentally. A removed flap was chosen to avoid additional flap sound sources in the experiments that accompany the numerical simulations. The additional flap sources would otherwise reduce the meaningful signal-to-noise ratio in acoustic far-field measurements. The clean chord length of the

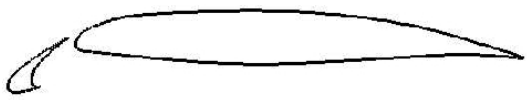

Fig. 1 Two-element slat configuration.

model used for the experiments is 0.4m. This paper presents acoustics results for 12^o and 13^o angle of attack. For these angles the suction peaks at the slat and main element leading edge closely reach the values that occur for a real 3 element high-lift airfoil under approach conditions with an angle of attack around 6^o. Spectra, directivities and the Mach number scaling law is studied using four different free flow Mach numbers (M=0.088,0.10,0.12,0.16). The acoustic effect of an add-on device that separates the clean flow from the recirculation region in the slat cove - termed slat cove cover - is studied.

3 Acoustic simulation techniques

3.1 Governing equations

For the acoustic simulations acoustic perturbation equations (APE-4) as introduced by Ewert & Schröder [6] are used. They are a modification of the genuine linearized Euler equations (LEE). The system solved for the pressure and velocity perturbations $(p', \vec{u}')$ is

$$\frac{\partial p'}{\partial t} + c_0^2 \nabla \cdot \left(\rho_0 \vec{u}' + \vec{u}_0 \frac{p'}{c_0^2} \right) = c_0^2 q_c \quad (1)$$

$$\frac{\partial \vec{u}'}{\partial t} + \nabla \left(\vec{u}_0 \cdot \vec{u}' \right) + \nabla \left(\frac{p'}{\rho_0} \right) = \vec{q}_m, \quad (2)$$

and exclude the non-acoustic modes otherwise apparent in the LEE. In eqns. (1) and (2) ρ_0, p_0, and $\vec{u}_0$ denote the density, pressure and velocity of the time averaged flow, respectively. Furthermore, $c_0 = \sqrt{\gamma p_0 / \rho_0}$ is the local speed of sound. Considering the source term on the right-hand side, the vorticity equation of the APE system becomes

$$\frac{\partial \vec{\omega}'}{\partial t} = \nabla \times \vec{q}_m. \quad (3)$$

Hence, the perturbation vorticity $\vec{\omega}' = \nabla \times \vec{u}'$, on the left-hand side is controlled by the right-hand side (RHS) source term. For the homogeneous system with all sources removed, the vorticity equation reduces to the statement that the vorticity remains constant (zero), i.e., the convective vorticity mode is not present.

The major source terms for turbulence related vortex sound can be identified [6, 7] to be

$$\vec{q}_m = -\left(\vec{\omega} \times \vec{u}\right)' = -\vec{\omega}_0 \times \vec{u}' - \vec{\omega}' \times \vec{u}_0 - \left(\vec{\omega}' \times \vec{u}'\right)', \quad (4)$$

where $(\ldots)' := (\ldots) - \overline{(\ldots)}$ denotes the perturbation of terms. A similar vortex source term appears in the acoustic analogies of Powell, Howe,

and Möhring [15, 9, 13]. The source term is computed from the velocity fluctuations provided by the stochastic method. The equations are integrated with the DLR CAA code PIANO applying the 4th order DRP scheme of Tam & Webb in space [17] and a LDDRK method [10] in time on block structured meshes.

3.2 Stochastic sound source model

A widely used [18] model function for space time-correlations of turbulence is based on Gaussian and exponential functions for the spatial and temporal correlations, respectively,

$$\mathcal{R}(\vec{y},\vec{r},\tau) = \hat{R}\,\exp\left[-\frac{\tau}{\tau_s} - \frac{\pi(\vec{r}-\vec{u}_c\tau)^2}{4l_s^2}\right]. \quad (5)$$

The parameters τ_s and l_s define respectively the correlation time- and length scales and $\hat{R}$ denotes the root-mean-square (RMS) value of the correlated quantity for vanishing separation space $\vec{r}$ and time τ. Taylor's hypothesis is taken into account by the convection velocity $\vec{u}_c$. For inhomogeneous turbulence τ_s, $\vec{u}_c$, l_s, and $\hat{R}$ depend on position $\vec{y}$.

The Random Particle Mesh (RPM) method [5, 4] is capable of generating spatially and temporally fluctuating quantities that reproduce target two-point space-time correlations of the type described by eq. (5), whereby local target values for the parameters are realized. To model turbulent velocity fluctuations some further improvements are introduced. The divergence-free conditions of vorticity related turbulence is taken into account by modeling a fluctuating streamfunction $\psi(\vec{y},t)$. Strictly solenoidal 2D perturbation velocities are deduced from this fluctuating streamfunction at each time instant via

$$u_i = \varepsilon_{ij}\frac{\partial\psi}{\partial y_j}, \quad (6)$$

where ε_{ij} denotes the 2D ε-tensor. In case of homogeneous isotropic turbulence the velocity correlations that follow from eq. (6),

$$\mathcal{R}_{ij}(\vec{r},\tau) = \overline{u_i(\vec{r}_1,t_1)u_j(\vec{r}_2,t_2)}, \quad (7)$$

match perfectly the complete velocity correlation tensor of isotropic turbulence for $\tau = 0$,

$$\mathcal{R}_{ij}(\vec{r},0) = \frac{2}{3}\bar{k}\left[\frac{f(r)-g(r)}{r^2}r_i r_j + g(r)\delta_{ij}\right]. \quad (8)$$

In the above expressions $\vec{r} = \vec{r}_1 - \vec{r}_2$ and $\tau = |t_1 - t_2|$ are the spatial and temporal separations between point 1 and 2. The separation distance is $r = |\vec{r}|$ and r_i is the ith component of vector $\vec{r}$. The turbulence kinetic energy is denoted by $\bar{k}$ and $f(r)$ and $g(r)$ denote the longitudinal and lateral correlation functions, respectively, which are connected for a two-dimensional problem through

$$g(r) = f(r) + r\frac{\mathrm{d}f(r)}{\mathrm{d}r}. \quad (9)$$

This neat feature to exactly realize homogeneous isotropic turbulence in the two-point correlations can be proven by considering the space-time correlations of the fluctuating streamfunction in this homogeneous case to be a pure function of the separation vector $\vec{r}$

$$\mathcal{R}_{\psi\psi}(\vec{r},\tau) = \overline{\psi(\vec{r}_1,t_1)\psi(\vec{r}_2,t_2)}. \quad (10)$$

The velocity correlations eq. (7) are connected via eq. (6) with the correlations eq. (10). By taking $\vec{r} = \vec{r}_1 - \vec{r}_2$ into account, the relationship is

$$\mathcal{R}_{ij} = -\varepsilon_{ik}\varepsilon_{jl}\frac{\partial^2\mathcal{R}_{\psi\psi}}{\partial r_k \partial r_l}. \quad (11)$$

Since ψ is generated by a procedure that realizes correlations of the type described by eq. (5), the correlation $\mathcal{R}_{\psi\psi}$ in eq. (11) can be expressed through the right-hand side of eq. (5), where the parameters are constants for the homogeneous problem. Next, the explicit expressions found for $\mathcal{R}_{ij}$ in the case $\tau = 0$ can be verified to have the formal shape defined by eq. (8), whereby the resulting longitudinal and lateral correlation functions furthermore satisfy eq. (9). To match quantitatively eq. (8) the amplitude $\hat{R}$ in eq. (5) has to set to

$$\hat{R} = \frac{4l_s^2\bar{k}}{3\pi}. \quad (12)$$

Then, the resulting longitudinal correlation function that follows from eq. (5) is a Gaussian,

$$f(r) = \exp\left(-\frac{\pi}{4}\frac{r^2}{l_s^2}\right), \qquad (13)$$

with an integral length scale directly determined by the parameter l_s,

$$L = \int_0^\infty f(r)\mathrm{d}r = l_s.$$

Hence, the parameters $\hat{R}$ and l_s in eq. (5) are directly linked via eqs. (12) and (13) to the turbulence kinetic energy and length scale as provided by RANS. The fluctuating streamfunction eq. (6) is generated by spatially filtering a white noise field, which is numerically approximated through a cloud of random particles in the resolved source region. To include the convection property as described by the Taylor hypothesis, the random particles are passively convected through the steady RANS mean-flow field. Frozen turbulence with a time scale $\tau_s \to \infty$ is achieved in eq. (5) if the random value of each particle is kept constant. If the random variables are allowed to change in time through a discretized Langevin equation, exponential time correlations according to eq. (5) can be realized. The approach can be extended to three dimensions and to include also anisotropic effects, e.g. as provided by Reynolds stress models. More details can be found in Ref. [4, 3].

4 Slat noise simulations

4.1 Statistical source features

The stochastic sound sources are generated on a user defined source patch. Fig. 2 presents the stochastic source patch at the slat in relation to the slat geometry and the CAA mesh of the slat reference geometry. It is believed that the major source of slat noise is due to the vortex structures that are generated in the slat cove shear layer and that convect past the slat trailing edge. To test this conjecture the source patch resolves the slat cove shear layer but omits the recirculation bubble in the slat cove. An important feature that has to be accomplished by the stochastic model

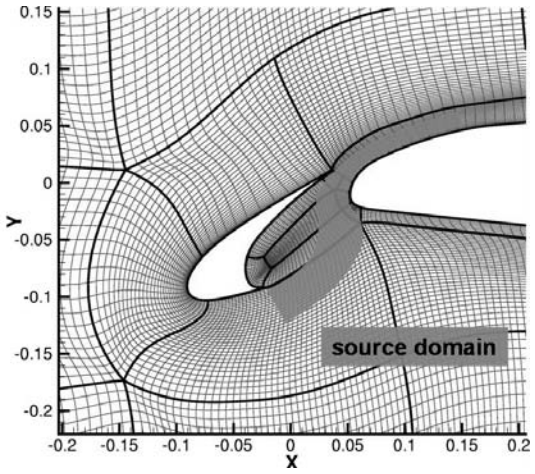

Fig. 2 Resolution of the slat shear-layer in the 2D test problem.

is the accurate resolution of the turbulence kinetic energy topology. To evidence this capability of the model, the Fig. 3 juxtaposes the RANS target solutions for the turbulence kinetic energy on the source patch to according results from the stochastic models. For this purpose, 20000 time levels of the stochastically generated velocities are sampled and averaged. One free parameter of the model is the number of random particles that are used to set up the fluctuating white-noise field. The influence of the number of random particles to resolve the source region is highlighted in Fig. 3. A total of 15000 and 45000 random particles, respectively, have been considered for this test. A fairly good realization of the turbulence energy for the energy topology as well as the absolute magnitudes is found. The streamtrace variations evidence a sufficient high number of particles employed, since no dependence of the statistical outcome on this parameter is visible.

4.2 Reference slat configuration

The computations in this paper are carried out with DLR's CAA code PIANO. The CAA grids used resolves the acoustic field in a $5c \times 5c$ box, where c denotes the main-element chord length. Based on a dimensional chord length $c = 0.4$m, the grid is sufficient to resolve frequencies up to 12kHz. The mesh resolution is enhanced in

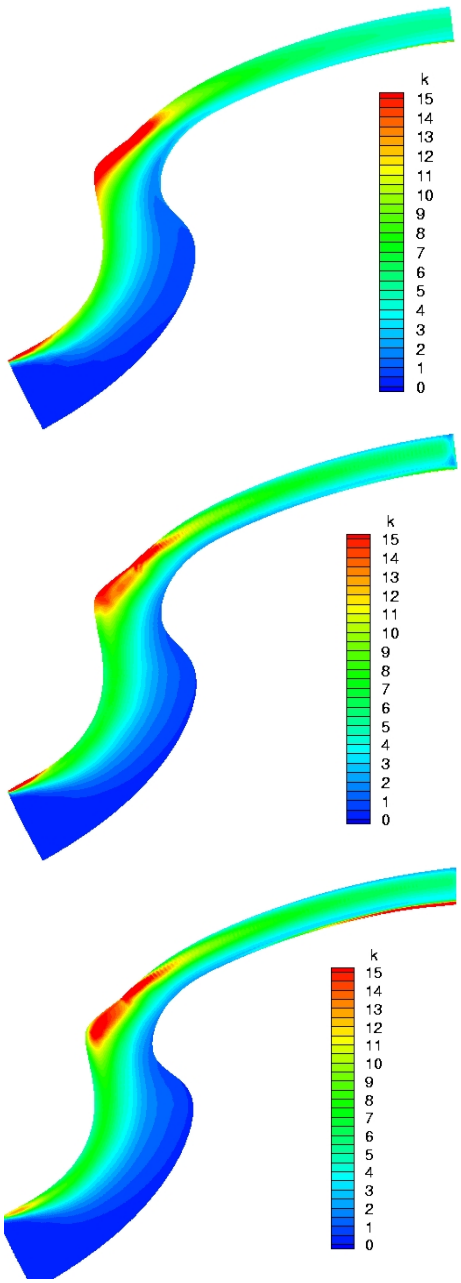

Fig. 3 RANS target distribution of the turbulence kinetic energy on the source patch (top) and results from stochastic realization; 15000 particle , middle; 45000 particle, bottom.

the slat-cove to resolve the estimated length scale of the source term properly. The RANS solution, which serves to prescribe the mean-flow and the turbulence features used by the stochastic method, is computed with DLR's flow-solver TAU on an unstructured mesh. A Menter SST turbulence model [12] with Kato-Launder modification is used. First, results for the reference two-element airfoil are presented for a mean-flow velocity of $M = 0.10$. Fig. 4 shows a snapshot of the unsteady pressure field generated at the slat. The acoustic fields roughly correspond to the one expected for a dipole source placed at the slat trailing edge with its axis normal to the slat chord. Fig. 5 presents a narrow band spectrum for an observer position above the slat. The computed narrow band spectrum for 0.4m chord length and 50m/s free flow velocity is juxtaposed to an acoustic far-field measurement that has been conducted by EADS Corporate Research Centre in DLR's Acoustic Windtunnel Braunschweig (AWB) as part of the German national project FREQUENZ. A qualitative good agreement in the spectral distributions is obtained.

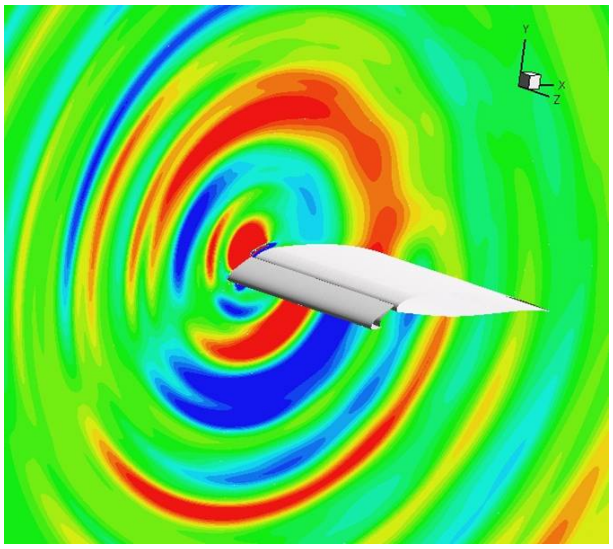

Fig. 4 APE/RPM simulation of broadband sound generation and radiation from the slat of a high-lift wing.

Fig. 6 compares an APE/RPM based 1/3-octave spectrum with the empirical slat-noise

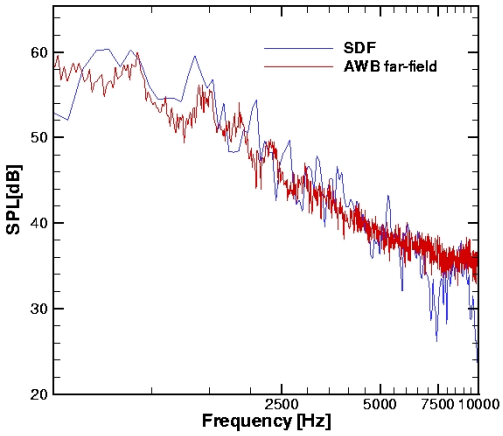

Fig. 5 Comparison of APE/RPM based narrow band spectrum with acoustic windtunnel measurement.

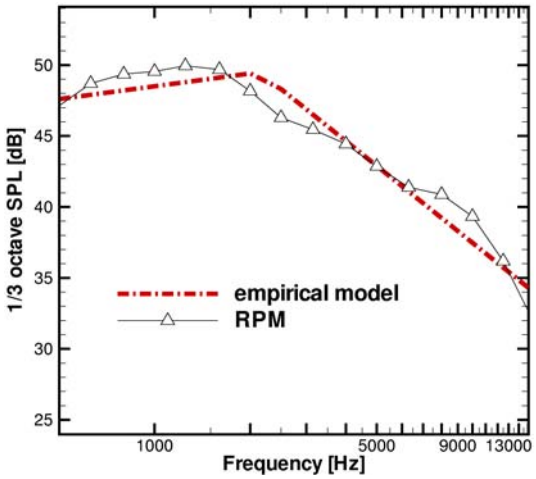

Fig. 6 Comparison of APE/RPM based 1/3-octave spectrum with the empirical model spectrum of Dobrzynski [2, 14].

model of Dobrzynski [2, 14]. The empirical slat-noise model is based on a generic spectrum that shows a typical peak frequency and falls off for higher frequencies according to a $f^{-1.8}$ law. The peak frequency depends on the slat deployment angle. The simulation reproduces these two distinct features, i.e., the peak frequency in a similar frequency range and the rate of decay of the spectrum for higher frequencies.

Fig. 7 compares directivities for two different frequencies (1kHz, 8kHz). The directivities are computed for a circle with center at the slat trailing edge and radius $1.5c$. For the lowest frequency of 1kHz, Fig. 7(top), the directivity in the upper half plane exhibits a directivity pattern, which is well known for trailing edge noise [7], see also Fig. 8 that depicts analytical solutions to the trailing edge directivity for different wavenumbers. However, compared to Fig. 8 the upper half plane pattern of Fig. 7(top) is mirrored at a vertical axis. In other words, it agrees with the directivity of an edge noise source located at the leading edge of a thin profile. Obviously, for the small frequencies the directivity is dominated by the scattering of the acoustic waves at the main-element. At higher frequency, Fig. 7(bottom), the directivity shows again a typical trailing edge pattern. But in this frequency range, the pattern is rotated such that the usual upstream direction points towards the ground. The direction roughly agrees with the slat chord angle. Hence, for the higher frequency range, the directivity is mostly affected by the slat geometry.

4.3 Mach number scaling law

Results of the Mach number scaling study are plotted in Fig. 9. Three different Mach numbers (0.088,0.12,0.16) are considered. From experiments it is deduced that the sound intensities scale according to a $M^{4.5}$ law for slat-noise, i.e., a slightly weaker growth compared to airfoil trailing edge noise, which can be shown analytically to scale with M^5. Usually the exponent can be attributed to several effects. First, the change of the convection velocity of vortical structures causes an increase in the radiated sound pressure. Second, the turbulent velocity fluctuations grow with increasing flow velocity. For analytical considerations it is usually assumed that the turbulent velocity fluctuation scale linearly with the freestream velocity. In the stochastic model the convection property is accounted for by convecting the random particles in the steady RANS mean-flow. The increase of turbulent fluctuations is taken into account in the model by the change of the turbulence kinetic energy levels, which are provided by the steady RANS solution. The

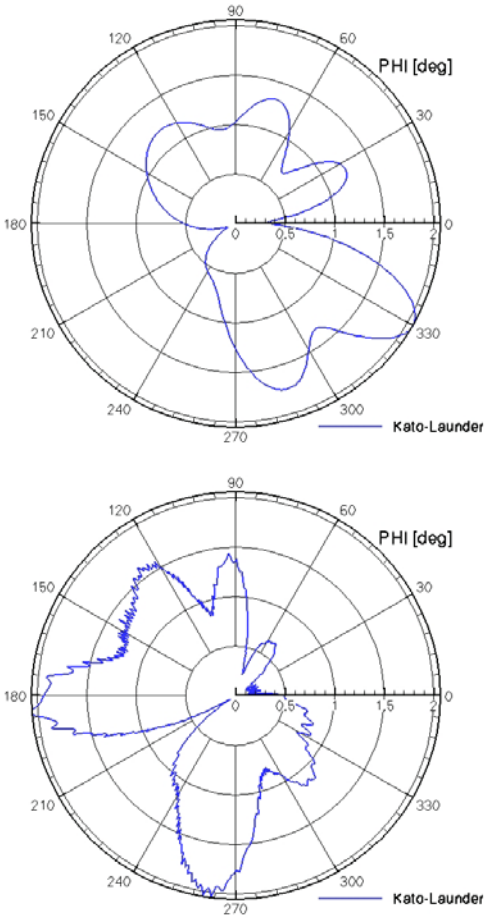

Fig. 7 Normalized directivities for the Menter SST model with Kato-Launder modification; the directivity circle is centered at the slat trailing edge and has radius $r = 1.5c$.

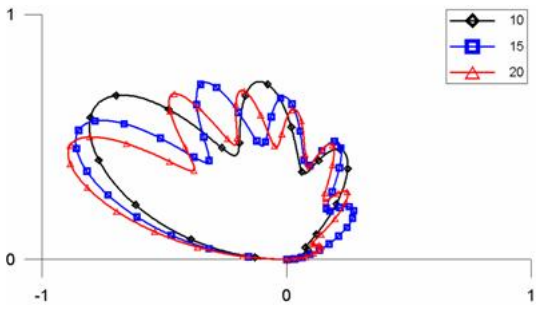

Fig. 8 Typical trailing-edge directivity of a semi-infinite flat plate for different wave-numbers.

Fig. 9 depicts the scaling of the root-mean square (RMS) fluctuating pressure for an observer position 1.5c below the slat trailing edge. A linear regression fit to the three data points yields a Mach number scaling law exponent of 1.54 for the RMS pressure. Just considering the first two Mach numbers the exponent changes to 1.65. Since the sound intensities scale with twice that value, one finds a scaling law with exponents between 3.08 and 3.3 for the considered 2D case. In [8] it was discussed that a 2D acoustic solution has to be corrected to take into account 3D sound radiation, which increases the scaling exponent by one. The correction formula was deduced to read

$$\widetilde{p}(0,R,\theta,\omega) \simeq \hat{p}(R,\theta,\omega)\frac{1+i}{2}\sqrt{\frac{kL^2}{\pi R}}. \qquad (14)$$

Here $\widetilde{p}$ denotes the 3D corrected (complex) spectral pressure and $\hat{p}$ is related to the 2D spectral pressure. L denotes a length scale of the problem, see Ref. [6]. Based on Taylor's hypothesis of convecting vorticity, the non-dimensionalizing of Eq. (14) yields with $k = \omega/c$, $\omega \propto u/\lambda_v$, where λ_v is the length scale of a vortical disturbance, the scaling

$$\widetilde{p} \propto M^{1/2}\,\hat{p},$$

i.e., the sound intensities in 3D scale with the power of the Mach number increased by one, compared to the 2D case. Accordingly, the corrected 3D scaling becomes 4.08 and 4.3, respectively, which is pretty close to the expected exponent.

4.4 Slat cove cover simulation

Finally the effect of a slat cove cover on the radiated sound field is studied. Fig. 10 shows the geometry of the slat cove cover and the topology of the CAA mesh in the vicinity of the slat. Fig. 11 juxtaposes a snapshot of the acoustic field for the clean slat (top) to that involving the slat cove cover (bottom). Since the pressure contour scaling was kept constant in both cases, it is evident from the field plots that the slat cove cover achieves a decrease in the acoustic amplitudes. This effect is also highlighted by comparing the

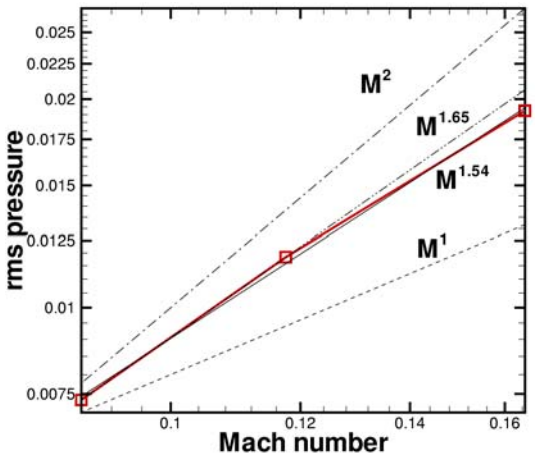

Fig. 9 Mach number scaling of root-mean-square pressure in an observer point at $\theta = 270^o$, 1.5 chord length below the slat trailing edge.

narrow band spectra for an observer position 1.5 clean chord lengths beneath the slat ($\theta = 270^o$), Fig. 12. In average a decrease of the sound pressure levels around $5dB$ is found for frequencies up to $8kHz$.

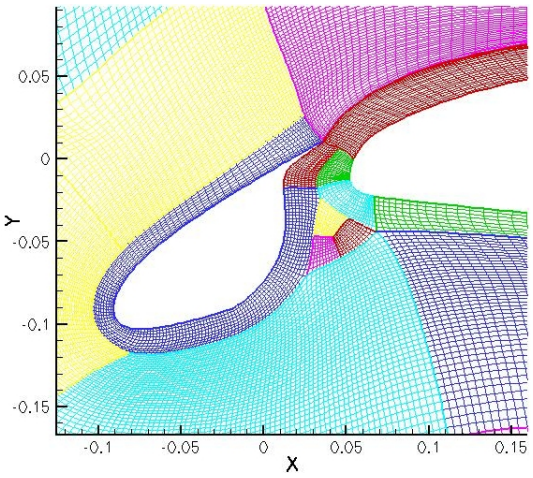

Fig. 10 CAA mesh to resolve the slat cove cover.

5 Summary and Conclusions

A low-cost CAA method has been applied to make slat noise predictions with an computational effort in the range acceptable for a design tool. The turbulence related slat-noise sources are modeled with a random particle mesh (RPM) method, which matches the statistical features of a steady RANS target solution quite closely. A modified two-element airfoil, consisting of a slat and a main element, is used for the slat noise predictions. The slat noise directivity found from the computations roughly corresponds to that of a dipole located at the slat trailing edge with its axis normal to the slat chord. The characteristics of narrow as well as 1/3-octave spectra agree with those found from measurements. The slat noise is found to scale with the 4.3 power of the Mach number. The effect of a slat cove cover was furthermore investigated. Reductions around 5dB in a range up to 8kHz (based on 0.4m clean chord length) are found in the narrow band spectra, clearly indicating a potential of slat cove fillers to reduce sound levels.

Acknowledgments

The authors would like to thank Prof. Költzsch of the technical university of Dresden for kindly providing the analytical solutions of the edge noise Green's function of Howe.

References

[1] G.K. Batchelor. *The Theory of Homogeneous Turbulence*. Cambridge University Press, 1960.

[2] W. Dobrzynski and M. Pott-Pollenske. Slat noise studies for farfield noise prediction. 2001. AIAA Pap. 2001-2158.

[3] R. Ewert. Broadband slat noise prediction based on caa and stochastic sound sources from a random particle-mesh (rpm) method. *submitted to Comp. and Fluids*.

[4] R. Ewert. Slat noise trend predictions using caa with stochastic sound sources from a random particle mesh (rpm) method. 2006. AIAA Pap. 2006-2667.

[5] R. Ewert and R. Emunds. Caa slat noise studies applying stochastic sound sources based on solenoidal digital filters. 2005. AIAA Pap. 2005-2862.

[6] R. Ewert and W. Schröder. Acoustic perturbation equations based on flow decomposition via source filtering. *J. Comput. Phys.*, 188:365–398, 2003.

[7] R. Ewert and W. Schröder. On the simulation of trailing edge noise with a hybrid LES/APE method. *Journal of Sound and Vibration*, 270:509–524, 2004.

[8] R. Ewert, Q. Zhang, W. Schröder, and J. Delfs. Computation of trailing edge noise of a 3d lifting airfoil in turbulent subsonic flow. 2003. AIAA Pap. 2003-3114.

[9] M. S. Howe. Contributions to the theory of aerodynamic sound, with application to excess jet noise and the theory of the flute. *J. Fluid Mech.*, 71(4):625 – 673, 1975.

[10] F. Q. Hu, M. Y. Hussaini, and J. L. Manthey. Low-dissipation and low-dispersion Runge-Kutta schemes for computational acoustics. *J. Comp. Phys.*, 124:177–191, 1996.

[11] R.H. Kraichnan. Diffusion by a random velocity field. *Physics of Fluids*, 13:22–31, 1970.

[12] F. Menter. Zonal two equation k-ω turbulence models for aerodynamic flows. 1993. AIAA Pap. 93-2906.

[13] W. Möhring. Modelling low mach number noise. In E.-A. Müller, editor, *Mechanics of Sound Generation in Flows*. Springer, 1979.

[14] M. Pott-Pollenske, W. Dobrzynski, H. Buchholz, B. Gehlhar, and F. Walle. Validation of a semiempirical airframe noise prediction method through dedicated a319 flyover noise measurements. 2002. AIAA Pap. 2002-2470.

[15] A. Powell. Theory of vortex sound. *Journal of the acoustical society of america*, 36/1:177–195, 1964.

[16] B.A. Singer, D.P. Lockard, and K.S. Brentner. Computational aeroacoustics analysis of slat trailing-edge flow. *AIAA Journal*, 38(9), 2000.

[17] C. Tam and J. Webb. Dispersion-relation-preserving finite difference schemes for computational acoustics. *J. Comp. Phys.*, 107:262–281, 1993.

[18] C.K.W. Tam and L. Auriault. Jet mixing noise from fine-scale turbulence. *AIAA Journal*, 37(2):145–153, 1999.

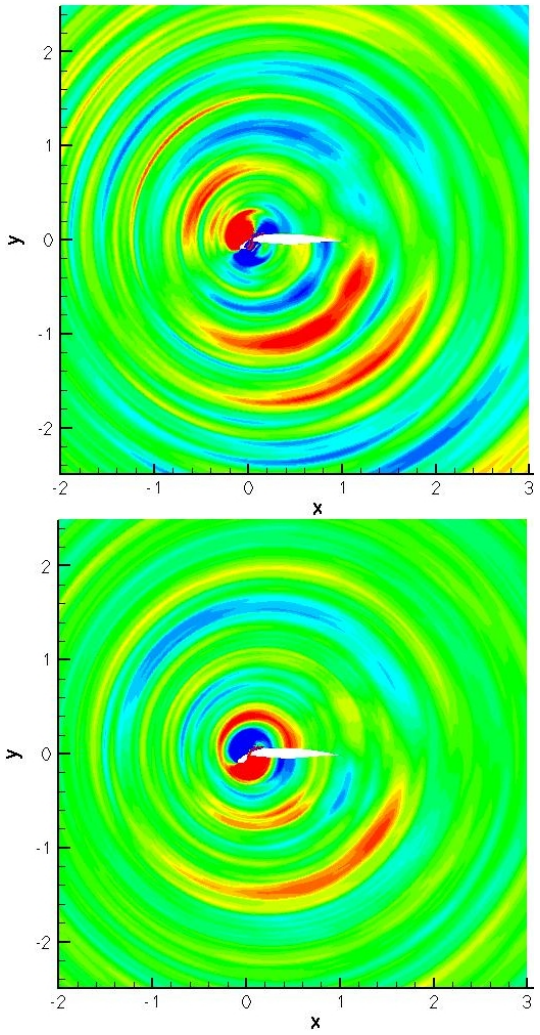

Fig. 11 Pressure contours of the reference (top) and the slat cove cover configuration (bottom).

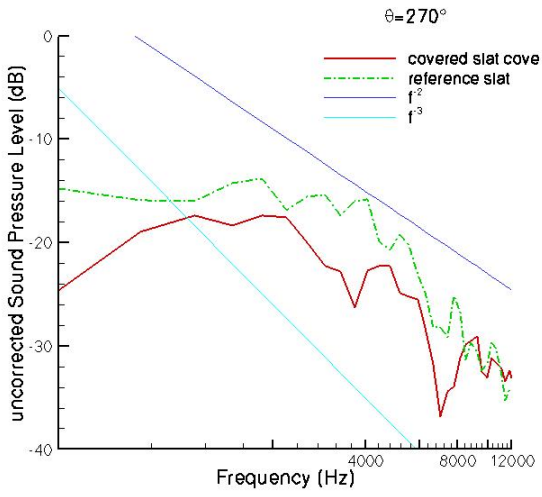

Fig. 12 Sound pressure spectra underneath the slat.